










From a novel synthesis method for bismuth tri-iodide nanoparticles to a solution-processed hybrid material: BiI₃-conducting polymer

Loengrid Bethencourt^{1,*} , Ivana Aguiar^{2,*} , María Pérez Barthaburu¹ , Daniela Oreggioni¹ , Ricardo Costa de Santana³ , Lauro June Queiroz Maia³ , and Laura Fornaro¹ 

¹Departamento de Desarrollo Tecnológico, Centro Universitario Regional del Este, Universidad de la República, Rocha, Uruguay

²Área de Radioquímica, Departamento Estrella Campos, Facultad de Química, Universidad de la República, Montevideo, Uruguay

³Instituto de Física, Universidade Federal de Goiás, Goiânia, Goiás, Brazil

Received: 16 May 2022

Accepted: 27 August 2022

Published online:

5 October 2022

© The Author(s), under exclusive licence to Springer Science+Business Media, LLC, part of Springer Nature 2022

ABSTRACT

We successfully synthesized two types of bismuth tri-iodide nanoparticles: uncapped (BiI₃) and capped with aniline (BiI₃_ani), in order to study their potential as inorganic semiconductor for an organic–inorganic hybrid material with poly(3-hexylthiophene-2,5-diyl) (P3HT). We developed a novel direct synthesis method that avoids ligand exchange (for BiI₃_ani), as well as the necessity of capping agent removal steps (for BiI₃) and the formation of secondary compounds obtained by other techniques. Additionally, we evaluated and compared the properties of solution-processed P3HT:nanoparticles layers with the film sequence ITO/PEDOT:PSS/P3HT:nanoparticles, where ITO is indium tin oxide and PEDOT:PSS is poly(3,4-ethylenedioxythiophene) polystyrene sulfonate. We analyzed the layers by UV–Vis spectroscopy, X-ray diffraction, focused ion beam scanning electron microscopy and photoluminescence analysis. We proved that aniline restricts the growth of nanoparticles and improves the processability of the material compared to nanoparticles without capping agent. We demonstrated that both types of nanoparticles can be successfully suspended in a solvent in which P3HT is soluble, improve the UV–Vis absorption of P3HT and interact with this polymer leading to an improved crystalline ordering on the blends compared to pristine P3HT layers. We also demonstrated that BiI₃ nanoparticles produce a nanoscopic mixture with P3HT and that it is possible to exploit the photoluminescence emission of P3HT:BiI₃_ani layers. Our results show that both types of nanoparticles can be good candidates for use in solution-processed organic–inorganic hybrid

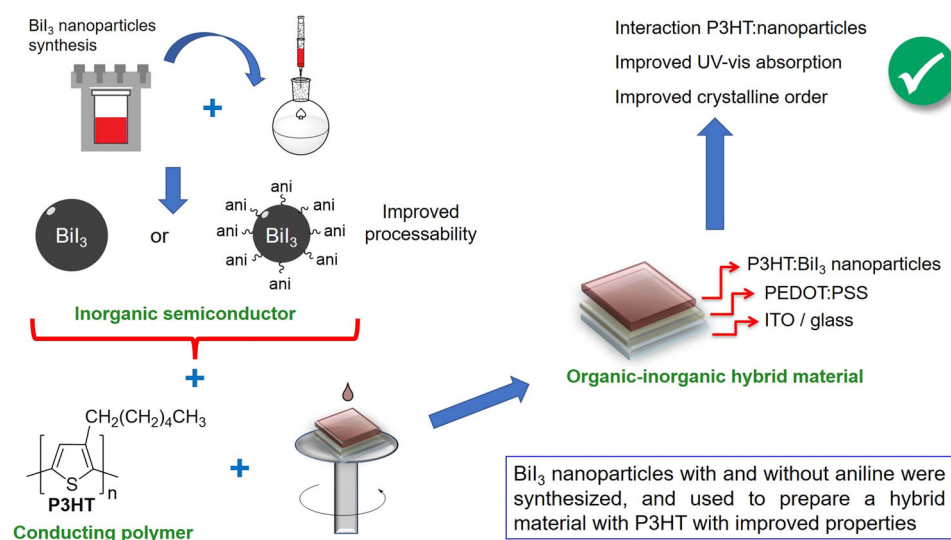
Handling Editor: Yaroslava Yingling.

Loengrid Bethencourt and Ivana Aguiar have contributed equally to this work and should be considered co-first authors.

Address correspondence to E-mail: loengridb@gmail.com; iaguiar@fq.edu.uy

material with P3HT, which could be employed for the fabrication of hybrid polymeric–inorganic solar cells with BiI₃ nanoparticles as electron acceptor and P3HT as electron donor.

GRAPHICAL ABSTRACT



Introduction

Organic–inorganic hybrids have emerged as a new class of highly versatile functional materials in which the organic and inorganic components combine their inherent physical properties and provide novel characteristics, increasing the range of electrical, optical, and morphological properties than those of the separated materials. Generally, organic molecules improve the optoelectronic properties of inorganic materials and provide low-cost and straightforward processability, such as spin coating, inkjet printing and roll-to-roll deposition, which are not always compatible with pure inorganic materials. In addition, they have high visible light absorption coefficients and offer the possibility of creating flexible and low-weight devices. At the same time, inorganic components offer useful optoelectronic properties, substantial mechanical toughness, heat resistance, and favorable optical properties given by the option to modify the bandgap by changing the sizes and

morphologies (due to the quantum confinement effect) [1–4].

The aforementioned characteristics allowed that organic–inorganic hybrids were considered as alternative to conventional materials for several applications, leading to a huge increase in research works related to them. For example, they demonstrated to have potential in the development of photoelectrochemical (PEC) and photovoltaic (PV) devices, a subject promoted by the necessity of finding new energy sources because of the considerable increase in the worldwide energy demand and the eventual depletion of resources used in non-renewable energy sources [5–9].

In the case of PV devices, besides all the alternatives that have been investigated with the final objective of achieving a more efficient energy conversion and/or reduce the cost in potential applications [10, 11] one of the possibilities that became very popular and include organic–inorganic hybrid material was the investigation of hybrid cells with mixtures of conjugated polymers as electron donors

and inorganic nanocrystals as electron acceptors. These cells are the so-called hybrid solar cells (specifically, hybrid polymer–inorganic solar cells) and investigations on this field have produced a much deeper understanding of optoelectronic interactions in organic–inorganic hybrid systems [12]. The favorite material of choice as conjugated polymer has been the poly(3-hexylthiophene-2,5-diyl) (P3HT), due to its improved optical absorption, better environmental stability and higher holes mobility, compared to some other studied polymers [13, 14]. The use of inorganic nanoparticles (Nps) in PV devices has some advantages, mainly related to the versatility of these materials, which can be synthesized in a great variety of sizes and morphologies according to the desired properties [15]. The properties of nanoscale materials (such as optical absorption/emission and electronic affinity) depend on their size. For example, as size decreases, the maximum absorption shifts toward blue due to a quantum confinement effect that changes the bandgap. In addition, inorganic Nps offer the advantage of being synthesized with morphology of spheres, rods, prisms, wires, tetrapods, hyperbranched nanocrystals, among others, with which not only the optical properties can be controlled but also, for example, solubility [16].

Choosing the appropriate inorganic semiconductor for organic–inorganic hybrids remains a challenge, because of the difficulty of finding a material with suitable properties, non-toxic, abundant, and with a simple and inexpensive synthesis procedure. Bismuth tri-iodide (BiI_3) has arisen as an excellent candidate given its remarkable properties. Their compound elements are earth abundant, and it has low toxicity. Also, it has a bandgap of 1.67 eV, which makes it a candidate for employing it as photoelectrode in PEC devices or as electron acceptor for solar cells, given the fact that P3HT and BiI_3 presents cascading energy levels [17–19]. In these last devices, the electrons coming from the dissociation of the excitons generated as a product of the photon absorption in the P3HT are transferred from the LUMO of this polymer (more negative) to the conduction band of BiI_3 (less negative) at the interface and are transported to the cathode for charge collection. The holes are transferred from the HOMO of P3HT to valence band of BiI_3 and are collected at the anode [19].

Moreover, Bi^{3+} has a large ionic radius, a more disperse valence band, and superficial intrinsic point defects because of its $6s^2$ lone pair of electrons, which consequently position the material among the defect-tolerant compounds [20].

BiI_3 has been widely studied as a material for X and gamma radiation detectors. Ionizing radiation detectors have been constructed from monocrystals, thick films, and lately from Nps [21–27]. Recently, given the drawbacks of lead perovskites for solar cells applications, as their toxicity and its rapid degradation, a great number of researchers have investigated BiI_3 films and perovskites as an alternative. For instance, BiI_3 has been electrodeposited and then transformed to the perovskite $(\text{CH}_3\text{NH}_3)_3\text{Bi}_2\text{I}_9$, and the same bismuth-based perovskite has been reported to provide power conversion efficiencies of 1.12% and 1.62% [28, 29]. Moreover, BiI_3 thin films have been obtained using different processing methods for photovoltaic applications [18, 30].

In light of the above, hybrid materials based on BiI_3 Nps have become relevant, because they will potentially show semiconductor character and interesting optical and electronic properties. However, not only the selection of the inorganic material is important, but also the nanoparticle coating which can influence the carrier transport and the compatibility processing with other materials. The nanoparticle synthesis generally involves the use of capping agents for controlling parameters as solubility, size, and shape. These molecules can remain in the nanoparticle surface and have a function or must be removed or exchanged for another useful molecule. Particularly, in organic–inorganic hybrid materials intended for practical applications, as in polymer–inorganic solar cells, the inorganic nanoparticle surface plays a crucial role [31]. For instance, the capping agents can passivate the surface by bonding the uncomplete dangling orbitals of Nps surface that can act as trapping sites of charge carriers [12]. Besides, the coating determines the ability of Nps to mix with the polymer (and the solvents used in the device fabrication process). Several studies were made on the influence of capping agents on the properties pointed out before. To mention, thiols and molecules containing amines and aromatic rings are among the most reported ones [31–34]. For example, Kumar et al. demonstrated that CdSe Nps capped with pyridine provides a low barrier distance that facilitates the charge transfer from the polymer to the Nps

in developing hybrid solar cells [33]. On the other hand, the solution processability of Nps is fundamental to obtain a homogeneous hybrid material. Pyridine and/or dodecanethiol were demonstrated to help in the suspension stability of SnS₂, CdSe and CdTe Nps in chloroform (solvent used to dissolve P3HT) [34–36]. In the case of Bi-based Nps such as BiI₃, the selection of the capping agent must contain a borderline base to stabilize the capping agent on the surface. This is explained because Bi³⁺ is a borderline acid, according to hard and soft Lewis acids and bases (HSAB) theory. This requisite leaves the amines (as pyridine and aniline) as potential candidates. In particular, aniline stabilized Nps with nonvolatile properties have been reported for memory applications, and BiI₃/PVAL (polyvinyl alcohol) nanocomposites have been studied for laser CUT-OFF optical devices [37–39].

In the present work, we successfully synthesized two kinds of Nps: BiI₃ without capping agent and BiI₃ capped with aniline (named herein after as BiI₃ and BiI_{3_ani}, respectively) in order to study their potential as inorganic semiconductor for an organic–inorganic hybrid material using P3HT as conjugated polymer. This allows us to evaluate and compare the properties of solution-processed P3HT:Nps layers using as a model the classical partial film sequence of a hybrid polymer–inorganic solar cell, namely ITO/PEDOT:PSS/P3HT:Nps, where ITO is indium tin oxide and PEDOT:PSS is poly(3,4-ethylenedioxythiophene) polystyrene sulfonate. We considered these two types of Nps due to the capping agent has the advantages mentioned above but it has also been reported cases in which a reduced insulating barrier given by the washing of capping agent led to an improved charge transfer between P3HT and Nps as well as an improved electron transport between Nps used in hybrid polymer–inorganic solar cells [12, 40]. We surmise that a small ligand as aniline could have the advantages of having a capping agent while avoiding its disadvantages.

We developed a novel direct synthesis method to obtain BiI_{3_ani} that prescind from ligand exchange so excluding its intrinsic limitations. Our synthesis method also allowed us the straightforward obtaining of BiI₃ without the necessity of washing steps. Additionally, for both types of Nps our method avoids the formation of secondary compounds obtained by other techniques, such as BiOI, Bi₅O₇I₉ and Bi₂O₃. On the other hand, we demonstrated that

both BiI₃ and BiI_{3_ani} can be good candidates for use in organic–inorganic hybrid material with P3HT, which could be used for the fabrication of hybrid polymeric–inorganic solar cells with Nps as electron acceptor and P3HT as electron donor.

Experimental

BiI₃ nanoparticles synthesis and characterization

We dissolved 2.25×10^{-3} mol of BiCl₃ (Merck, 98%) in 10 mL of HCl 4.5 M (Dorwil, analytical grade), and 13.7×10^{-3} mol of NaI (Mallinckrodt, analytical reagent) in 5 mL of distilled water. We added the NaI solution to the BiCl₃ solution dropwise. The final orange solution was transferred to a 20 mL home-made Teflon-lined stainless-steel autoclave, heated at 180 °C for 8 h, and then cooled naturally to room temperature. After the hydrothermal treatment, a strong red solution was obtained. We injected 3.5 mL of that solution into 100 mL of distilled water, both at room temperature. We prepared samples without (BiI₃) and with a capping agent (BiI_{3_ani}); when a capping agent was used, 250 μL of freshly distilled aniline (Mallinckrodt, ACS) was added to the distilled water before the injection of bismuth and iodide precursors solution. We isolated the obtained black precipitates from the solution by centrifugation, washed them with chloroform repeatedly (Dorwil, analytical grade), and dried at 40 °C for 24 h. We chose chloroform because is possible to wash the product without decomposition. Moreover, we could suspend Nps in the solvent very well and it is compatible with the procedure for obtaining P3HT and nanoparticles blends.

We studied the identity of samples by X-ray diffraction (XRD) in a PANalytical Empyrean diffractometer equipped with a Cu(Kα) source ($\lambda = 1.5418 \text{ \AA}$). The diffractograms were obtained at room temperature in a Bragg–Brentano configuration. We used diffuse Fourier-transform infrared spectroscopy (FTIR) to study the presence of the capping agent, in a Shimadzu IRPrestige-21 with a DiffusIR Pike Technology accessory. We employed transmission electron microscopy (TEM) with a Jeol 2100 microscope to study size and morphology. Bandgap was determined by UV–visible (UV–Vis) spectroscopy using a Shimadzu 2600

spectrophotometer with a diffuse reflectance sphere. Besides, we analyzed the stability and solubility of suspensions by turbidimetry, using a PerkinElmer Lambda 35, in chloroform as solvent. To do this we made absorbance measurements at 150 and 475 nm (wavelengths where none of the species absorb) every 15 min, from 0 to 60 min. In the stability study the Nps suspension was left at rest all the time, while in the solubility study the suspension was sonicated just before each absorbance measurement.

P3HT:nanoparticles blend layers fabrication and analysis

We separately prepared a stock suspension of BiI_3 -ani or BiI_3 Nps and a stock solution of P3HT (electronic grade, Rieke Metals, Inc.) in chloroform (99.98%, Dorwil) with sonication for 5–10 min at room temperature. For most studies, P3HT:Nps blends were obtained by combining appropriate amounts of both stock mixes in order to get a final suspension of 20 mg Nps mL^{-1} and 1:2 m-m proportion of P3HT:Nps after sonication at room temperature for 60 min.

We fabricated the P3HT:Nps layers considering the film sequence of a hybrid polymer–inorganic solar cell, namely ITO/PEDOT:PSS/P3HT:Nps. First, unpatterned ITO coated glass substrates (Delta Technologies Ltd, 20 mm \times 20 mm, 1.1 mm of thickness, sheet resistance 4–10 $\Omega \text{ cm}^{-2}$) were rinsed with type I grade water and cleaned by successive ultrasonication at 60 °C for 10 min in (1) deep cleaning detergent (Hellma Analytics, Hellmanex® III) solution in type I grade water, (2) type I grade water and (3) 2-propanol (Merck, $\geq 99.8\%$), leaving them in a fresh serving of 2-propanol. Rinses were made with sufficient type I grade water between each change of cleaning substance. We then dried the substrates with a nitrogen stream and treated with UV/ozone for 15 min using a UV/ozone cleaner Ossila L2002A2. Subsequently, we transferred all cleaned substrates to a glove box under a nitrogen atmosphere. All layers were deposited under this atmosphere using a spin coater Laurell Technologies WS-650 Hz-23NPP-UD-3. We deposited the PEDOT:PSS layer onto ITO film by dynamic spin coating 35 μL of aqueous dispersion of the commercial reagent (Ossila Ltd, HTL Solar Formulation, AI 4083), previously filtrated by 0.45 μm syringe filter, at 5000 rpm for 45 s followed by heating at 120 °C for 10 min. Finally, films of P3HT:Nps

were prepared by dynamic spin coating 150 μL of blend suspension onto a PEDOT:PSS film at 700 rpm for 3 min and then annealing at 150 °C for 15–30 min.

It is worth mentioning that most of the work involving the manipulation of P3HT was done inside a glove box under a nitrogen atmosphere. In cases where it was necessary to handle the P3HT (or any mixture containing this substance) outside the glove box, we took care to protect it from white light.

In order to study if there is any interaction between P3HT and Nps, we analyzed the blend layers by UV–Vis spectroscopy and XRD. These studies were complemented through focused ion beam scanning electron microscopy (FIB-SEM) and photoluminescence (PL) analysis. The UV–Vis spectroscopy was also performed to make an optical characterization of the blend layers and XRD allowed us to analyze the crystalline behavior of the blend layers. In cases in which P3HT layers were included for comparative reasons, we deposited these layers onto ITO/PEDOT:PSS system using an utterly analogue procedure as stated above. UV–Vis studies were performed employing a PerkinElmer Lambda 35 UV–Vis spectrophotometer. XRD analyses were performed in the same equipment and under the same conditions used for nanoparticle characterizations. FIB-SEM images were taken with a ZEISS Sigma 300 microscope from Carl Zeiss Microscopy Research Solutions, and the PL emission spectrum was obtained using a Fluorolog®-3 spectrofluorometer, FL3-221 Horiba-Jobin Yvon.

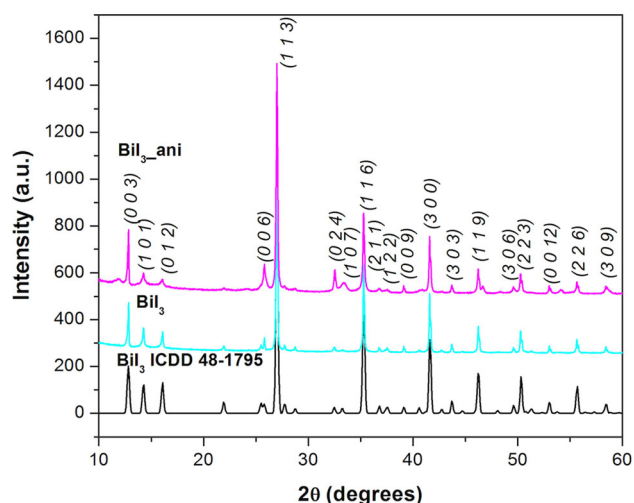


Figure 1 XRD patterns of BiI_3 -ani and BiI_3 samples, compared with the BiI_3 ICDD file 48-1795.

Results and discussion

BiI₃ nanoparticles synthesis and characterization

XRD patterns show that bismuth tri-iodide was obtained in all cases. Figure 1 shows the obtained patterns indexed to the rhombohedral BiI₃ phase (ICDD file 48-1795). A slight peak broadening can be observed in the sample BiI₃_ani, as in the peaks at 25.9° and 33.4°, evidencing that the sample is composed of nanometric crystallites.

The novel synthesis method developed in this work avoids the formation of secondary compounds obtained using other techniques, such as BiOI, Bi₅O₇I₉ or Bi₂O₃. These compounds result from the poor dissolution of bismuth precursors, which are difficult to dissolve in water, and that hydrolyze with humidity [41]. Bi³⁺ ion is susceptible to hydrolysis even at pH as low as 1–2 forming basic salts [42]. However, BiCl₃ dissolves in strong acids in the presence of the common ion Cl⁻. In our procedure, we used a method that employs acid medium combined with hydrothermal treatment, which allows the complete dissolution of all reactants, avoiding the formation of undesired compounds. After the hydrothermal treatment, all the ions are in aqueous solution. Considering that the BiI₃ solubility product constant ($K_{sp} = 7.7 \times 10^{-19}$) is a billion times smaller than K_{sp} for BiCl₃ (2.45×10^{-7}) and BiOI (2.1×10^{-11}), when we inject the solution rapidly into the water, pH increases and BiI₃ precipitates [43–45].

Concerning morphology, we obtained Nps of 638 nm and 200 nm average size in BiI₃ and BiI₃_ani samples, respectively, as can be seen in TEM images in Fig. 2. Moreover, the narrowest size dispersion was obtained in the BiI₃_ani sample. In the BiI₃ sample, we obtained wider size distribution and poor morphology uniformity. From these images we can asseverate that aniline plays an important role restricting the size of these Nps. Moreover, in BiI₃_ani sample we also found smaller nanoparticles, between 1 and 9 nm. These results show that aniline restricts the growth of nuclei, improving morphology homogeneity and size distribution. It also enhances the suspension of nanostructures in organic solvents such as chloroform (as we demonstrated later), which is necessary to obtain a good mixture with the polymer in an organic–inorganic hybrid material. The high-resolution image of one of these particles and its

respective Fourier Transform shows that they are crystalline, and they grow mainly in the [1 1 3] direction. This growth orientation has been already observed in other works, and it coincides with the highest intensity peak in the BiI₃ X-ray diffractogram [27].

When we compare our results with bismuth tri-iodide Nps synthesized by other authors, we can see that our Nps are smaller in size than the Nps synthesized by a wet chemical route but without the hydrothermal step and with higher amounts of aniline [37, 38], as can be seen in Table 1. Furthermore, when we attempted to increase the aniline concentration, we obtained orange oxide bismuth compounds in all cases. XRD analysis of these samples can be seen in Fig. S1 (Supplementary Information). Besides, as pyridine is a known capping agent for Nps to be included in hybrid materials, we tried to use it in our synthesis. However, we did not obtain bismuth tri-iodide, but we obtained orange oxide bismuth compounds no matter the amount of pyridine employed.

Regarding to the study related to the presence of aniline as the capping agent through diffuse FTIR spectroscopy the results are shown in Fig. 3, when the spectrum of BiI₃_ani and BiI₃ can be compared. The first difference we saw is the broadband at 2982 cm⁻¹ and the band at 2592 cm⁻¹ in the sample BiI₃_ani. These bands can be attributed to the N–H stretching of the amine salt. We could not identify the bands corresponding to the N–H stretching (between 3300 and 3500 cm⁻¹) and the N–H bending (between 1650 and 1580 cm⁻¹) of the primary amine in the same sample. However, we can conclude that aniline is present in the sample because of the band at 1493 cm⁻¹, corresponding to the vibration of the aromatic C–C bond, and the bands at 744, 690, 999, 1026, 1079, 1102, 1188, 1286, and 1324 cm⁻¹, corresponding to C–H bonds. Given the previous evidence, we can state that aniline is linked to the BiI₃ Nps. We also can assume that aniline is linked to the Nps by the amine segment, because all the bands corresponding to the primary amine are missing [46].

The bandgap of the samples was obtained by UV–Vis spectrometry, estimating the values with the Tauc equation:

$$\alpha hv = A(hv - E_g)^n \quad (1)$$

where α is the absorption coefficient, hv corresponds to the photon energy, A is a constant, and n denotes

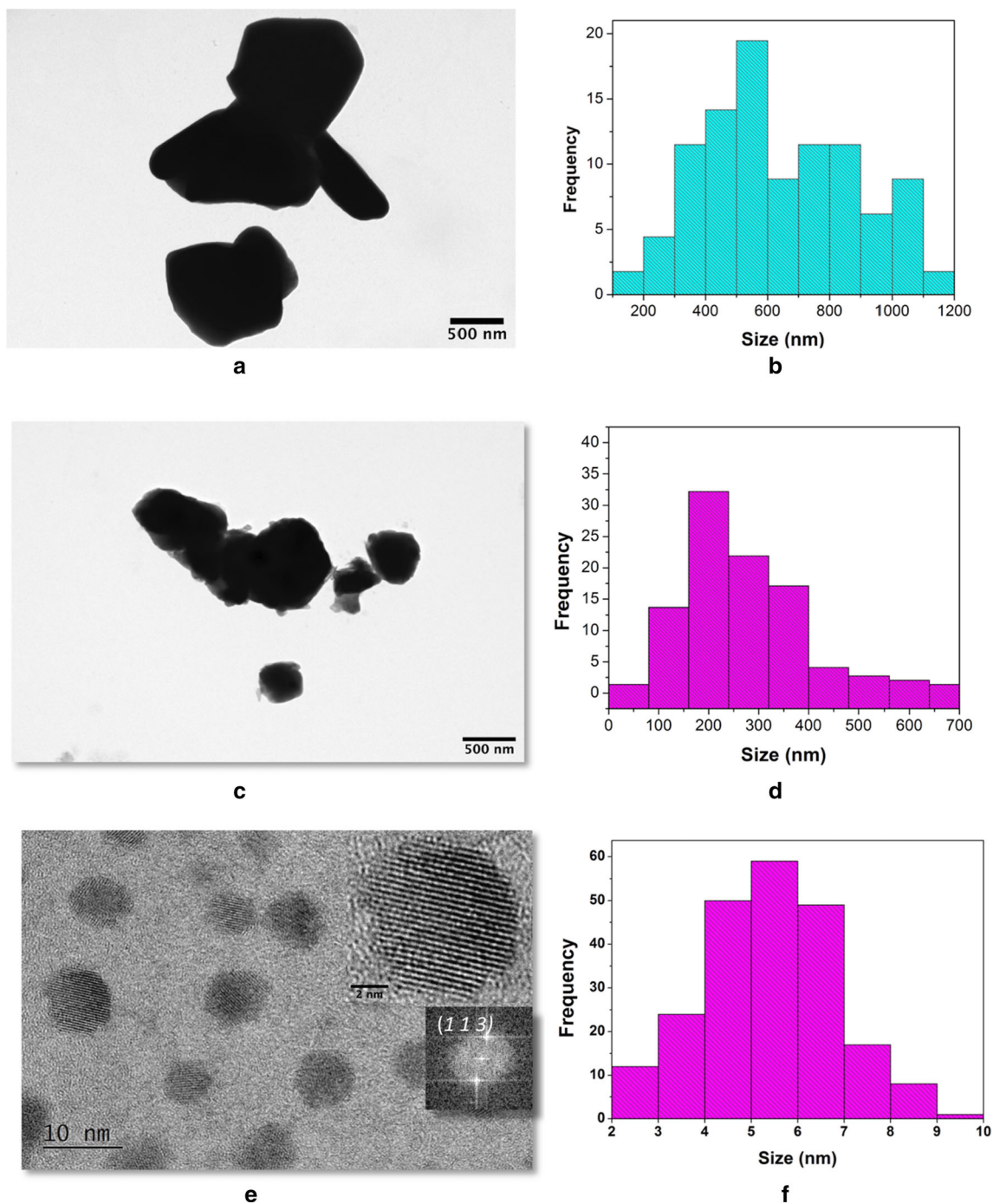


Figure 2 TEM images of **a** particles of average size 638 nm in the BiI_3 sample, **b** respective histogram, **c** particles of average size 200 nm in size in the BiI_3 _ani sample, **d** respective histogram,

e particles of 5 nm average size in the BiI_3 _ani sample, inset: HRTEM image of a particle with the Fourier Transform of that image, **f** histogram of particles in **e**.

Table 1 Comparison of nanoparticles results with similar works

Source	Method	Smallest size	Amount of aniline
This work	Hydrothermal + precipitation	5 nm	2.6×10^{-6} M
Ghosh et al. [37]	Wet chemical	17–20 nm	1.0 M
Perla et al. [38]	Wet chemical	18 nm	1.0 M

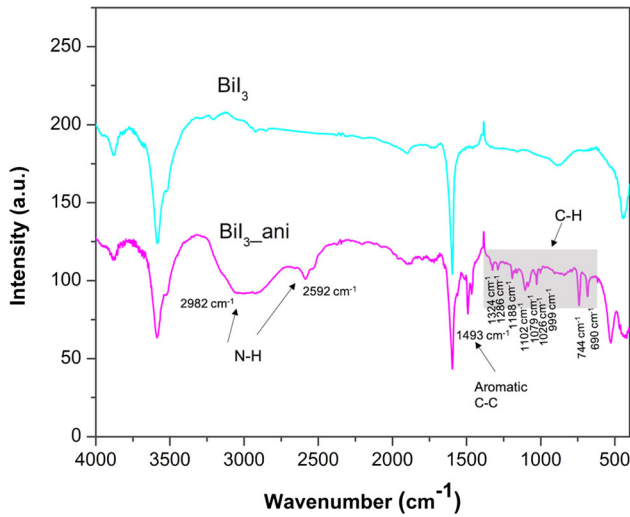


Figure 3 FTIR spectra of BiI₃_ani and BiI₃ samples.

the nature of the transition, being $n = 1/2$ for a direct transition and $n = 2$ for an indirect transition. The Tauc plots for both samples can be observed in Fig. 4. We obtained bandgap values of (1.79 ± 0.04) eV and (1.81 ± 0.07) eV for BiI₃ and BiI₃_ani samples, respectively, considering that BiI₃ is an indirect semiconductor [17]. There is no significant difference between both values; therefore, we can state that both samples are equivalent from the light absorption perspective. The values are also in agreement with the bandgap obtained for BiI₃ in previous works (1.67 eV for single crystals, 1.79 eV for films grown by physical vapor deposition, and 1.80 eV for solution-processed films [17, 20]).

On the other hand, the results of stability and solubility tests are displayed in Fig. 5. In the stability tests, the absorbance diminishes with time in both samples, but in much greater proportion for the BiI₃ one, which indicates a higher decantation for these particles. According to the solubility tests, for the

suspension with the BiI₃_ani the absorbance remains mainly constant (with a slight decrease of 8% if we compare the initial value with the one at 60 min). For the BiI₃ sample, we observe a more pronounced decrease, which indicates that the particles dissolve in a higher proportion. Therefore, after 60 min the absorbance of the BiI₃ sample decreased 62% compared with the initial value. These results also explain the non-linear decrease observed for the BiI₃ sample in the stability test (Fig. 5a), given the fact that not only the decantation of the particles is occurring but also its dissolution in chloroform.

Analysis of P3HT:nanoparticles layers

Figure 6 shows the normalized UV–Vis absorption spectra of P3HT:Nps and pristine P3HT layers.

It is seen that both the blend layers and the pristine polymer layer absorb light mainly in the 450–650 nm visible range. The results coincide with that reported in the literature for layers of regioregular P3HT or mixtures that contain it, where this polymer has a strong and wide π – π^* absorption band between 450 and 650 nm, which indicates an extensive π electrons delocalization [47].

All spectra are highly structured and exhibit the common vibrational modes of absorption peaks of regioregular P3HT layers, which implies the presence of highly ordered structures. These vibrational modes, that correspond to the excited electronic state, were designated as signal 1, 2 and 3, respectively, in the table inserted in Fig. 6. These results are in agreement with that reported in the literature [48] for the absorption spectra of regioregular P3HT films, which present two differentiated parts: the one with the shortest wavelength (higher energy) is most likely associated with intra-chain states related to

Figure 4 Tauc plot of BiI₃ and BiI₃_ani samples.

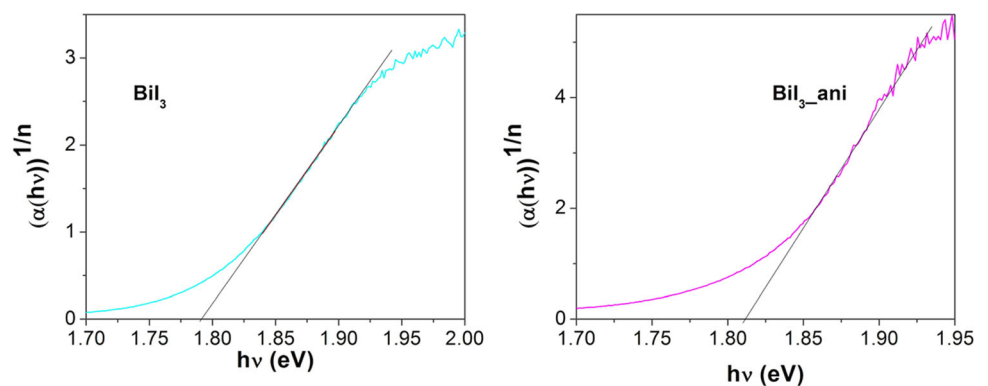


Figure 5 **a** Stability test, and **b** solubility test performed to BiI_3 and $\text{BiI}_3\text{-ani}$ samples in chloroform.

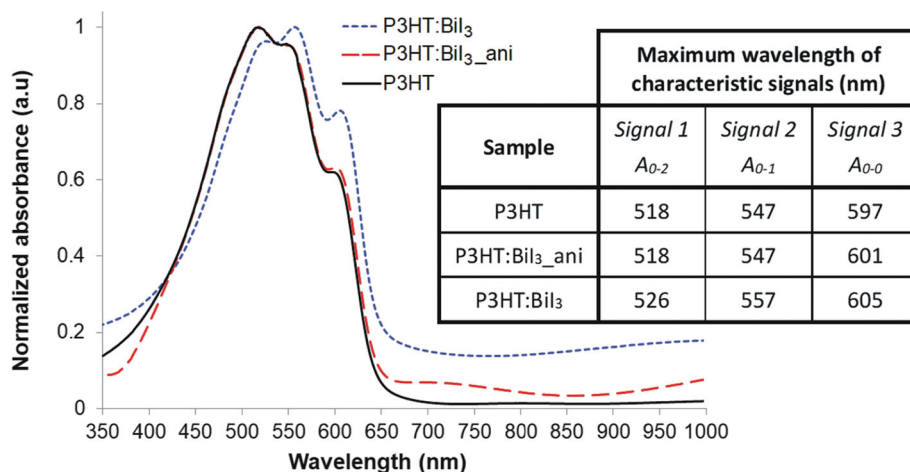
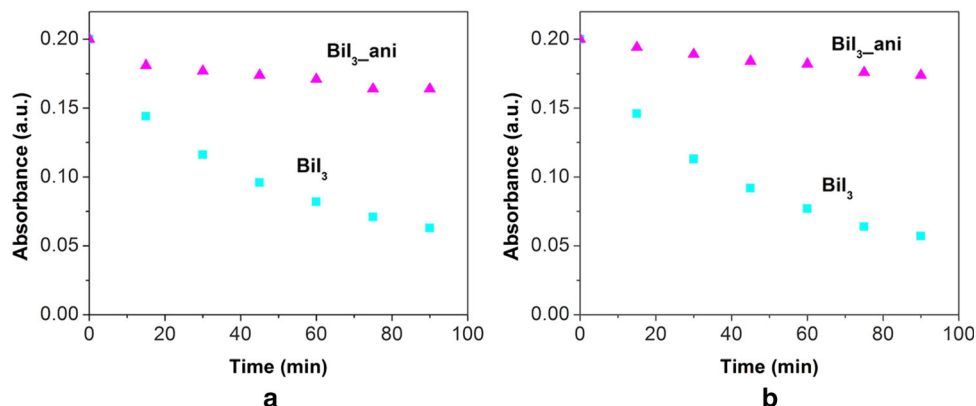


Figure 6 Normalized UV–visible absorption spectra of P3HT:BiI₃_ani, P3HT:BiI₃ and pristine P3HT layers deposited onto glass-ITO/PEDOT:PSS system. The blank consisted of a layer of PEDOT:PSS deposited onto an ITO substrate. We

prepared P3HT:Nps blends from suspensions of 20 mg Nps mL⁻¹ and 1:2 m-m proportion of P3HT:Nps in chloroform. P3HT layer was prepared with the same procedure and P3HT concentration of the blends.

disordered chains in the amorphous part of the film, while the part with higher wavelength (lower energy) denotes H-type aggregates that interact weakly in the crystalline regions of the layer. Thus, we can assign the signals observed in the spectra to the A_{0-2} and A_{0-1} intra-chain excitation transitions and the A_{0-0} transition of π - π interaction between P3HT chains, for signals 1, 2 and 3, respectively, with signal 3 being the result of π -stacking within the more ordered regions of the polymer layer and suggesting that the chain packing is compact in all samples [49–51].

It is necessary to point out that in all cases the contribution of the Nps in the optical absorption of the active layer is perceived. Thus, we found that the spectra of the blend layers tends to increase below 350 nm and that the baseline increases compared to pristine P3HT. Additionally, the intensity of signal 3 for the blend layers is greater than that of pristine

P3HT and the absorption spectra of the blend layers are wider than that corresponding to pristine P3HT, as was previously reported for P3HT:CdSe blends that were used in solar cells [52].

Furthermore, for the P3HT:BiI₃ blend layer there is a change in the relative intensities of signals 1, 2 and 3, as well as a redshift of these signals when compared to those of pristine P3HT. We attribute this hypsochromic shift to the presence of π -stacked aggregates in which the twist of the P3HT chain is strongly restricted, leading to planar molecules with extended conjugation, which is not necessarily a sign of a ground state interaction, but is often due to an increase in electron delocalization along the chain [48]. This redshift, which implies a greater conjugation length, leads to an increase in the light absorption capacity of P3HT with the inclusion of nanostructures. These results could suggest that the

conformation of the P3HT is being modified by its interaction with the Nps, i.e., the incorporation of the latter modifies the structure of the polymer, promoting ordering and, therefore, greater crystallinity. Moreover, this order increases the interactions between the P3HT chains in the mixtures in comparison with the pristine polymer. This has been previously reported, for example, for active layers of P3HT with ZnO Nps doped with Ho^{3+} , where it is concluded that the nanostructures induced an improvement in the structural ordering of the hybrid heterostructure [53].

The aforementioned results look promising when considering the use of the P3HT:BiI₃ blend as the active layer of a hybrid polymer–inorganic solar cell. Similarly, from an analysis by FIB-SEM (Fig. 7) it was clearly perceived that there are BiI₃ Nps within the matrix of P3HT forming a nanoscopic mixture with it, which is highly positive and desirable when considering the use of P3HT:Nps blends as active layers on PV devices.

On the other hand, for the case of P3HT:BiI₃_ani blend layers we can observe from Fig. 6 that the spectrum of the mixture tends to increase below 350 nm, is slightly wider than that of pristine P3HT and the baseline increases, but there is no significant change with the addition of Nps.

In order to deepen the above and determine if BiI₃_ani Nps could be useful, we used three

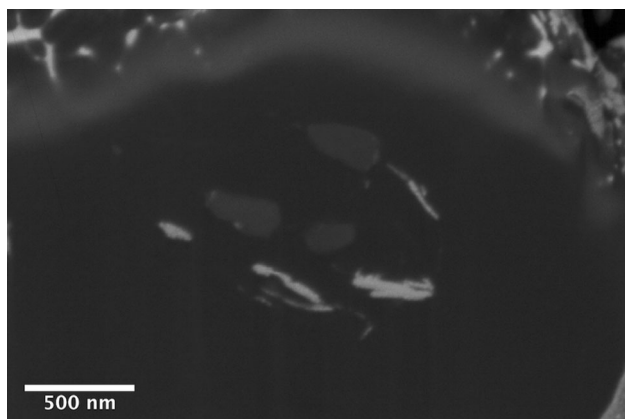


Figure 7 Backscattered electrons (BSE) FIB-SEM cross-sectional image of a P3HT:BiI₃ layer deposited onto glass-ITO/PEDOT:PSS with an electron high tension of 1.4 kV. The light areas correspond to BiI₃ and the dark areas to P3HT since the detection included backscattered electrons. We prepared the blend from suspensions of 20 mg Nps mL⁻¹ and 1:2 m-m proportion of P3HT:Nps in chloroform. Images courtesy of ZEISS Research Microscopy Solutions acquired with the ZEISS Sigma 300.

approaches: (1) comparison of spectra of P3HT:BiI₃_ani layers using the same amount of P3HT with different amount of Nps to determine if there is any influence of Nps in P3HT absorption band; (2) PL analysis to study a possible autoabsorption within the layer, and (3) analysis of the results of the H-type aggregate model proposed by Spano et al. [54]. This model provides quantitative estimates on the degree of excitonic coupling within the aforementioned H-type aggregates, a parameter that is related to the average conjugation length and the crystalline quality of the layers and that finally conditions the properties of the devices made with such layers (more details of this model in Supplementary Information).

With regard to approach (1), Fig. 8 shows that the intensity of the P3HT UV–Vis absorption band increases when the amount of Nps in the blend layer increases. This is highly desirable for application in solar cells as it is an indication of a “coupling” between the polymer and the Nps, and because it implies that the active layer would have a greater capacity to absorb light. This is in agreement with what is reported in the literature, for example, in mixtures of P3HT with Nps of CdSe with thioglycolic acid as capping agent [55], of CdSe with tributylphosphine oxide as capping agent, of ZnO doped with Ho^{3+} [53], or with PC71BM as electron acceptor in solar cells, among others [49, 56].

For approach (2), the results of PL analysis can be seen in Fig. 9. They show that it is possible to exploit the PL emission centered at 450 nm, as it can be absorbed by the layer and promote extra charge carrier generation.

Finally, the results of the H-type aggregates model [approach (3)] can be seen in Table 2, which also includes what corresponds to BiI₃ for comparative reasons.

When we analyze the values of bandwidth of the free excitons within the crystalline domains (W) it is seen that they are lower in the blend layer compared to pristine P3HT. These results suggest that there is an increase in the length of conjugation and the order of the chains (and, therefore, a higher crystalline quality of the layers could be expected) with the inclusion of Nps. This fact coincides with that reported in the literature, for example, for solar cells made with blends of P3HT and ZnO nanostructures doped with Ho^{3+} [50]. As the functional properties of solar cells depend to a large extent on this order of the P3HT chains, the results obtained seem

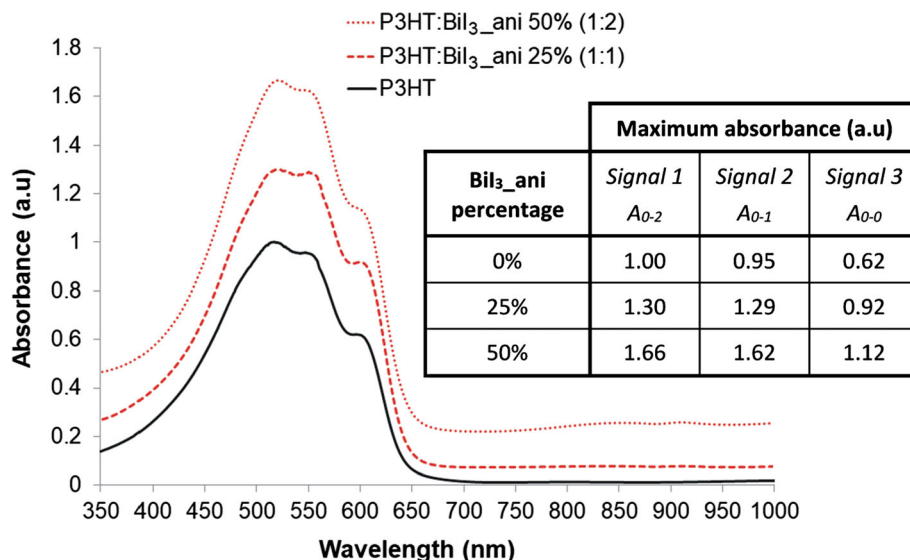


Figure 8 UV–visible absorption spectra of P3HT:BiI₃_ani layers deposited onto glass-ITO/PEDOT:PSS system, with the same concentration of P3HT and different concentrations of BiI₃_ani nanoparticles. The percentages correspond to volume percentages

of Nps suspension in each blend. The P3HT:BiI₃_ani proportions are also presented. The concentration of P3HT was 10 mg mL⁻¹ in all samples and that of BiI₃_ani ranged from zero (pristine P3HT) to 20 mg mL⁻¹ [P3HT:BiI₃_ani 50% (1: 2)].

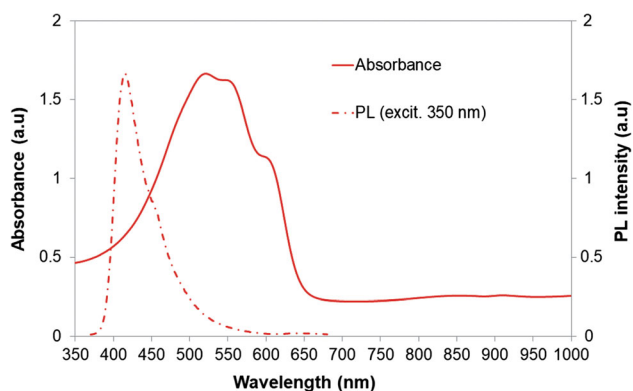


Figure 9 Absorption spectrum and PL emission spectrum of P3HT:BiI₃_ani layer deposited onto glass-ITO/PEDOT:PSS system. Excitation wavelength = 350 nm. P3HT:Nps blend was prepared from suspensions of 20 mg Nps mL⁻¹ and 1:2 m-m proportion of P3HT:Nps in chloroform.

promising when considering the use of both, BiI₃ and BiI₃_ani Nps for hybrid solar cells with P3HT, since it is known that the effective length of polymer conjugation in the thin films of active layer is a critical parameter to define the general performance in optoelectronic devices [57]. In fact, it has been reported that local crystallinity may play a key role in the efficiency of long-range charge pair generation in hybrid polymer–inorganic heterojunctions [51].

We deepened in the study of the crystalline behavior of the blends with the XRD analysis that follows. Figure 10 shows the powder diffractograms for layers of pristine P3HT and P3HT:Nps blends, as well as the diffractograms of the BiI₃ and BiI₃_ani powder samples. Powder diffractograms of ITO and PEDOT:PSS are included as we deposited all layers onto glass-ITO/PEDOT:PSS system.

In general, for the case of the blends we can observe that there is an appropriate phase

Table 2 Results for the calculation of the bandwidth of the free excitons within the crystalline domains (*W*) and comparison of pristine P3HT versus P3HT:BiI₃ blend layers

Sample	Absorbance (a.u)		<i>W</i> (meV)	Decrease in <i>W</i> (%)
	Signal 3 <i>A</i> ₀₋₀	Signal 2 <i>A</i> ₀₋₁		
P3HT	0.620	0.956	117.28	–
P3HT:BiI ₃ _ani	0.631	0.952	111.73	5.0
P3HT:BiI ₃	0.781	1.000	68.72	70.7

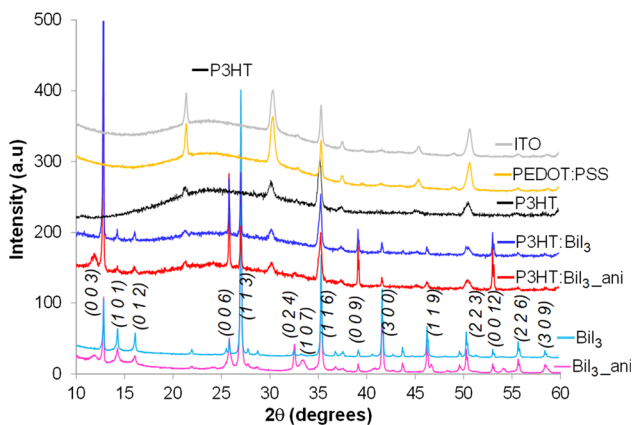


Figure 10 Powder diffractograms of P3HT, P3HT:BiI₃ and P3HT:BiI_{3_ani} layers deposited onto glass-ITO/PEDOT:PSS system, and of powder samples of BiI₃ y BiI_{3_ani}. All diffractograms were normalized with respect to the signal $2\theta = 35.2^\circ$ and they are displayed offset on the intensity axis for better visualization. We prepared the blends from suspensions of 20 mg Nps mL⁻¹ and 1:2 m-m proportion of P3HT:Nps in chloroform. P3HT layer was prepared with the same procedure and P3HT concentration of the blends.

composition within the layers. As expected, in the cases of the mixtures, P3HT and the glass-ITO/PEDOT:PSS system, an amorphous region is observed, given by a wide halo between approximately 17° and 35° .

To deepen the analysis of this section, we separated the results according to three approaches: (1) comparison of P3HT:Nps blends diffractograms with those corresponding to pure Nps, (2) comparison of P3HT:Nps blends diffractograms with those corresponding to pristine P3HT, and (3) determination of relative crystallinity degree of P3HT:NP layers.

(1) Comparison of P3HT:Nps blends diffractograms with those corresponding to pure Nps:

In both cases (BiI_{3_ani} versus P3HT:BiI_{3_ani} and BiI₃ versus P3HT:BiI₃), there is no significant difference in the width of the signals corresponding exclusively to BiI₃ or BiI_{3_ani}, which implies that P3HT does not impair the crystalline ordering within the Nps. Similarly, there is no significant change in the angles at which the different reflections appear (Table S1, Supplementary Information). Thus, there is no significant change in the interplanar distances when comparing each of the signals from the nanoparticle diffractograms with those corresponding to the blends. This implies that no changes occur in the crystalline structure of the Nps with the incorporation of P3HT.

Another interesting aspect to mention is that corresponding to relative intensities (Table S2, Supplementary Information). In general, the relative intensities are greater in mixtures than in pure Nps. This constitutes an improvement in the crystalline ordering of the layers as the width of the signals remains with no change.

Additionally, we determined if there is any preferential orientation of the Nps in blend layers. In order to do this, we calculated the texture coefficients shown on Table 3 (see Supplementary Information for more details).

Considering that TC values greater than 1 indicate a preferential orientation of the crystals/grains in the samples [58], the values obtained for our layers indicate that in all cases there is a preferential crystallographic orientation in the [0 0 3] direction, as have been previously reported for bismuth tri-iodide Nps synthesized by hydrothermal method and electron beam irradiation [34, 59]. Our results imply that the preferential orientation observed in the Nps is retained in the blends.

(2) Comparison of P3HT:Nps blends diffractograms with those corresponding to pristine P3HT:

Figure 11 shows powder diffractograms of P3HT, P3HT:BiI₃ and P3HT:BiI_{3_ani} layers deposited onto glass-ITO/PEDOT:PSS system.

The results are indicative of well-organized interplanar structures. There is also the [1 0 0] diffraction at 5.3° , which has been reported for P3HT layers and implies a crystalline phase with lamellar structure in which the P3HT chains adopt an edge-on orientation (Fig. S2a) [52, 60, 61]. This is stated since the position of the latter signal is associated with a separation of the lattice of 1.64 nm, which corresponds to the distance between the main chains of P3HT and the periodicity along the direction of alkyl groups (Fig. S2b). Thus, our results suggest that the orientation of the P3HT chains is parallel to the direction of growth, with the plane of the thiophene rings perpendicular to the substrate [62–64]. It is worth mentioning that we did not observe the diffraction peaks corresponding to P3HT crystallites with other orientations (for example, both the main chain of the polymer and the side chains parallel to the substrate). This is likely due to improved P3HT π - π stacking [65] and is a similar result to that reported in the literature for nanocomposite of carbonaceous graphene oxide and P3HT [52], Br-P3HT films [60, 63], pristine P3HT-films and powder [61, 62, 64], among others. It could

Table 3 Texture coefficients corresponding to representative signals of the diffractograms of P3HT:nanoparticles blends and pure nanoparticles

Miller index	P3HT:BiI ₃ _ani		BiI ₃ _ani		P3HT:BiI ₃		BiI ₃	
	RelI. ^a (%)	TC ^b	RelI. ^a (%)	TC ^b	RelI. ^a (%)	TC ^b	RelI. ^a (%)	TC ^b
0 0 3	100	3.86	23.95	1.37	100	3.73	20.38	1.20
1 1 3	8.27	0.05	100	0.97	16.47	0.10	100	1.00
3 0 0	1.25	0.03	25.05	0.87	3.31	0.07	25.65	0.92
1 1 9	1.03	0.05	10.72	0.80	1.96	0.10	11.3	0.87

^aRel I. = relative intensity

^bTC = texture coefficient

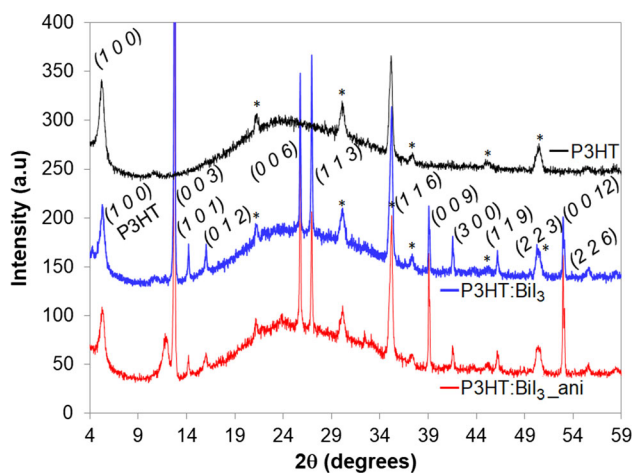


Figure 11 Powder diffractograms of P3HT, P3HT:BiI₃ and P3HT:BiI₃_ani layers deposited onto glass-ITO/PEDOT:PSS system. Signals with asterisks correspond to the substrate. All diffractograms were normalized with respect to the signal $2\theta = 30.1^\circ$ and they are displayed offset on the intensity axis for better visualization. We prepared the blends from suspensions of 20 mg Nps mL⁻¹ and 1:2 m-m proportion of P3HT:Nps in chloroform. P3HT layer was prepared with the same procedure and P3HT concentration of the blends.

be produced by the sonication treatment of P3HT blend solutions as it was previously reported for P3HT solutions and films [65].

In all cases, there is also a lower intensity peak at 10.6° , corresponding to the second order reflection whose Miller index is [2 0 0]. On the other hand, the third-order reflection [3 0 0] at approximately 15.9° is observed in the diffractogram of pristine P3HT as a signal with very little intensity. In the case of

Table 4 Comparison of the angles and interplanar distances corresponding to [1 0 0] diffraction for pristine P3HT and P3HT:nanoparticles blends

Sample	2θ (°)	D (nm)	P3HT versus blends D difference (nm)
Pristine P3HT	5.23	1.69	–
P3HT:BiI ₃ _ani	5.41	1.63	– 0.06
P3HT:BiI ₃	5.32	1.66	– 0.03

mixtures, at this angle there is a superimposition of the signal corresponding to BiI₃Nps (observed in Fig. 10) and the one from P3HT.

Finally, when we compare the angles at which diffraction [1 0 0] occurs and, therefore, the interplanar distances, we obtained the results of Table 4. These results indicate that the incorporation of BiI₃ within the P3HT matrix does not generate significant structural perturbations in the direction of the stacking of the alkyl chains of the polymer. This is probably due to the fact that Nps are incorporated into the P3HT matrix through the zone corresponding to the π - π stacking of polythiophene chains which is also in agreement with what was said above regarding the improvement in P3HT π - π stacking.

(3) Determination of relative crystallinity degree of P3HT:Nps layers:

In this section, we made an estimation of the degree of relative crystallinity of the layers, considering the diffractograms of the P3HT and the mixtures P3HT:BiI₃ and P3HT:BiI₃_ani with the subtracted background. For this, we did the processing in exactly the same way for all the samples, taking into account that the information can be extracted approximately from the following equation:

$$\text{Crystallinity}(\%) = \frac{A_{\text{crystalline}}}{A_{\text{crystalline} + \text{amorphous}}} \times 100 \quad (2)$$

where $A_{\text{crystalline}}$ is the total area of crystalline signals and $A_{\text{crystalline} + \text{amorphous}}$ is the total area of all signals.

The results are presented in Table 5, below.

Table 5 Relative crystallinity of P3HT and P3HT:BiI₃ blend layers

Sample	$A_{\text{crystalline}}$ (a.u)	$A_{\text{crystalline+amorphous}}$ (a.u)	Crystallinity (%)
P3HT (reference)	482.41	800.04	60
P3HT:BiI ₃	1197.40	1521.63	79
P3HT:BiI ₃ _ani	1355.97	1789.61	76

As can be seen, the relative crystallinity is higher in the case of blends compared to pristine P3HT. This agrees with what was discussed before, where we suggested that the incorporation of Nps in the P3HT matrix promotes ordering (and, therefore, greater crystallinity). In addition, it also agrees with that reported in the literature for blends of P3HT:CdS Nps, where it is stated that a higher content of CdS results in a more crystalline character, which would favor the transfer of electrons in a hybrid polymer–inorganic solar cell made with this blend as active layer [51].

Conclusions

We developed a novel synthesis method to obtain bismuth tri-iodide Nps without the formation of secondary phases, with and without aniline as capping agent. For BiI₃_ani our method leaves out ligand exchange so excluding its intrinsic limitations, and for BiI₃ it allows the straightforward obtaining of the Nps without the necessity of capping agent removal steps. We proved that aniline not only restricts the growth of the Nps, but also allows a better mixture between the Nps and the solvent used further to fabricate the polymer–Nps layers, improving therefore, the processability of the material.

We also demonstrated that both BiI₃ and BiI₃_ani Nps are good candidates for use in solution-processed organic–inorganic hybrid material with P3HT, which could be employed for the fabrication of hybrid polymeric–inorganic solar cells with Nps as electron acceptor and P3HT as electron donor. This is due to Nps can be successfully suspended in a solvent in which the polymer is soluble (chloroform), improve the magnitude of polymer absorption in part of the UV–Vis range and interact with the polymer in the mixtures improving the crystalline ordering of the blends compared to pristine P3HT layers. We also demonstrated that there are BiI₃ Nps within the matrix of P3HT forming a nanoscopic mixture with it

and that it is possible to exploit the PL emission of P3HT:BiI₃_ani layers, as it can be absorbed by the layer and promote extra charge carrier generation.

Our results can also be a starting point for future studies related to a deeper understanding of optoelectronic interactions in organic–inorganic hybrid systems, which can lead to very interesting practical applications.

Acknowledgements

The authors thank to A. Olivera for TEM images, H. Bentos Pereira and D. Ferreira for XRD measurements, Laboratorio de Físicoquímica, Facultad de Química, Universidad de la República for the FTIR equipment, Dr. Jorge Gancheff for the UV–Vis equipment, ZEISS Research Microscopy Solutions for FIB-SEM images. We also thank Agencia Nacional de Investigación e Innovación (ANII) and Programa de Desarrollo de las Ciencias Básicas (PEDECIBA) from Uruguay, and Coordenação de Aperfeiçoamento de Pessoal de Nível Superior—Brasil (CAPES)—Finance Code 001, the National Institute of Photonics—INFO (INCTs program) and Sisfóton-MCTI supported by CNPq, CAPES, FACEPE and FAPEG from Brazil, for funding. The research that gives rise to the results presented in this publication received funds from ANII under the codes POS_NAC_2012_1_9262, POS_NAC_2015_1_109609, FSE_1_2011_1_6771 and FCE-1-2016-127077.

Author's contribution

LB and IA contributed equally to this work. LB and IA performed the major part on sample preparation, conceptualization and formal analysis. DO performed stability and solubility tests. RS and LQM performed photoluminescence spectra. LB, IA and MPB wrote the original draft. RS, LQM and LF

reviewed the manuscript. MPB and LF had a major role in funding acquisition. LF supervised the work.

Declarations

Conflict of interest There are no conflicts to declare.

Supplementary Information: The online version contains supplementary material available at <http://doi.org/10.1007/s10853-022-07703-w>.

References

- [1] Wang Y, Liu K, Mukherjee P et al (2014) Driving charge separation for hybrid solar cells: photo-induced hole transfer in conjugated copolymer and semiconductor nanoparticle assemblies. *Phys Chem Chem Phys* 16:5066–5070. <https://doi.org/10.1039/c3cp55210a>
- [2] Duché D, Bencheikh F, Ben DS et al (2014) Optical performance and color investigations of hybrid solar cells based on P3HT:ZnO, PCPDTBT:ZnO, PTB7:ZnO and DTS(PTTh2)2:ZnO. *Sol Energy Mater Sol Cells* 126:197–204. <https://doi.org/10.1016/j.solmat.2014.03.049>
- [3] Pérez Barthaburu M, Galain I, Aguiar I et al (2017) Hybrid β -HgS nanoparticles and P3HT layers for solar cells applications. *Nano Struct Nano Objects* 10:15–21. <https://doi.org/10.1016/j.nanos.2017.02.001>
- [4] Barma SV, Rondiya SR, Jadhav YA et al (2020) Structural, optoelectronic, and photoelectrochemical investigation of CdSe nanocrystals prepared by hot injection method. *ES Mater Manuf* 11:50–56. <https://doi.org/10.30919/esmm5f1040>
- [5] Mana PM, Bhujbal PK, Pathan HM (2020) Fabrication and characterization of ZnS based photoelectrochemical solar cell. *ES Energy Environ* 12:77–85. <https://doi.org/10.30919/esee8c1021>
- [6] Vairale P, Sharma V, Bade B et al (2020) Melanin sensitized nanostructured ZnO photoanodes for efficient photoelectrochemical splitting of water: synthesis and characterization. *Eng Sci* 11:76–84. <https://doi.org/10.30919/es8d0023>
- [7] Mahadik SA, Patil A, Pathan HM et al (2021) Thionaphthoquinones as photosensitizers for TiO₂ nanorods and ZnO nanograin based dye-sensitized solar cells: effect of nanostructures on charge transport and photovoltaic performance. *Eng Sci* 14:46–58. <https://doi.org/10.30919/es8d1160>
- [8] Ibrayev N, Omarova G, Seliverstova E et al (2021) Plasmonic effect of Ag nanoparticles on polymethine dyes sensitized titanium dioxide. *Eng Sci* 14:69–77. <https://doi.org/10.30919/es8d1168>
- [9] Elayappan V, Murugadoss V, Fei Z et al (2020) Influence of polypyrrole incorporated electrospun poly(vinylidene fluoride-co-hexafluoropropylene) nanofibrous composite membrane electrolyte on the photovoltaic performance of dye sensitized solar cell. *Eng Sci* 10:78–84. <https://doi.org/10.30919/es5e1007>
- [10] Chen C, Xie X, Yang M et al (2021) Recent advances in solar energy full spectrum conversion and utilization. *ES Energy Environ* 11:3–18. <https://doi.org/10.30919/esee8c416>
- [11] Akinoglu BG, Tuncel B, Badescu V (2021) Beyond 3rd generation solar cells and the full spectrum project: recent advances and new emerging solar cells. *Sustain Energy Technol Assess* 46:101287. <https://doi.org/10.1016/j.seta.2021.101287>
- [12] Gao F, Ren S, Wang J (2013) The renaissance of hybrid solar cells: progresses, challenges, and perspectives. *Energy Environ Sci* 6:2020–2040. <https://doi.org/10.1039/c3ee23666h>
- [13] MacLachlan AJ, Rath T, Cappel UB et al (2015) Polymer/nanocrystal hybrid solar cells: influence of molecular precursor design on film nanomorphology, charge generation and device performance. *Adv Funct Mater* 25:409–420. <https://doi.org/10.1002/adfm.201403108>
- [14] Yuan J, Gallagher A, Liu Z et al (2015) High-efficiency polymer–PbS hybrid solar cells via molecular engineering. *J Mater Chem A* 3:2572–2579. <https://doi.org/10.1039/C4TA03995E>
- [15] Sawant JP, Deokate RJ, Pathan HM, Kale RB (2021) Spray pyrolytic deposition of CuInS₂ thin films: properties and applications. *Eng Sci* 13:51–64. <https://doi.org/10.30919/es8d1147>
- [16] de Freitas JN, de Carvalho Alves JP, Nogueira AF (2018) Hybrid solar cells: effects of the incorporation of inorganic nanoparticles into bulk heterojunction organic solar cells. In: Souza FL, Leite ER (eds) *Nanoenergy*. Springer International Publishing, Cham, pp 1–68
- [17] Podraza NJ, Qiu W, Hinojosa BB et al (2013) Band gap and structure of single crystal BiI₃: resolving discrepancies in literature. *J Appl Phys* 114:033110. <https://doi.org/10.1063/1.4813486>
- [18] Hamdeh UH, Nelson RD, Ryan BJ et al (2016) Solution-processed BiI₃ thin films for photovoltaic applications: improved carrier collection via solvent annealing. *Chem Mater* 28:6567–6574. <https://doi.org/10.1021/acs.chemmater.6b02347>
- [19] Wright M, Uddin A (2012) Organic–inorganic hybrid solar cells: a comparative review. *Sol Energy Mater Sol Cells* 107:87–111. <https://doi.org/10.1016/j.solmat.2012.07.006>
- [20] Brandt RE, Kurchin RC, Hoye RLZ et al (2015) Investigation of bismuth triiodide (BiI₃) for photovoltaic applications. *J Phys Chem Lett* 6:4297–4302. <https://doi.org/10.1021/acs.jpcclett.5b02022>

- [21] Lintereur AT, Qiu W, Nino JC, Baciak J (2011) Characterization of bismuth tri-iodide single crystals for wide band-gap semiconductor radiation detectors. *Nucl Instrum Methods Phys Res Sect A Accel Spectrom Detect Assoc Equip* 652:166–169. <https://doi.org/10.1016/j.nima.2010.12.013>
- [22] Matsumoto M, Hitomi K, Shoji T, Hiratate Y (2002) Bismuth tri-iodide crystal for nuclear radiation detectors. *IEEE Trans Nucl Sci* 49:2517–2520. <https://doi.org/10.1109/TNS.2002.803883>
- [23] Cuña A, Noguera A, Saucedo E, Fornaro L (2004) Growth of bismuth tri-iodide platelets by the physical vapor deposition method. *Cryst Res Technol* 39:912–919. <https://doi.org/10.1002/crat.200410276>
- [24] Cuña A, Aguiar I, Gancharov A et al (2004) Correlation between growth orientation and growth temperature for bismuth tri-iodide films. *Cryst Res Technol* 39:899–905. <https://doi.org/10.1002/crat.200410274>
- [25] Ikeda M, Oka Y, Mori K, Atsuta M (2004) Study of dark current blocking layer for BiI₃ X-ray detector film. In: *IEEE Nuclear science symposium conference record 2004*, vol 7, pp 4520–4523. <https://doi.org/10.1109/NSSMIC.2004.1466888>
- [26] Aguiar I, Kröger S, Fornaro L (2009) Bismuth tri-iodide polycrystalline films for X-ray direct and digital imagers. *Nucl Instrum Methods Phys Res Sect A Accel Spectrom Detect Assoc Equip* 610:332–334. <https://doi.org/10.1016/j.nima.2009.05.184>
- [27] Aguiar I, Olivera A, Mombrú M et al (2017) Novel bismuth tri-iodide nanostructures obtained by the hydrothermal method and electron beam irradiation. *J Cryst Growth* 457:244–249. <https://doi.org/10.1016/j.jcrysgro.2016.06.024>
- [28] Banik A, Bohannan EW, Switzer JA (2020) Epitaxial electrodeposition of BiI₃ and topotactic conversion to highly ordered solar light-absorbing perovskite (CH₃NH₃)₃Bi₂I₉. *Chem Mater* 32:8367–8372. <https://doi.org/10.1021/acs.chemmater.0c02304>
- [29] Jain SM, Edvinsson T, Durrant JR (2019) Green fabrication of stable lead-free bismuth based perovskite solar cells using a non-toxic solvent. *Commun Chem* 2:91. <https://doi.org/10.1038/s42004-019-0195-3>
- [30] Zhu Y, Zhang Q, Kam M et al (2020) Vapor phase fabrication of three-dimensional arrayed BiI₃ nanosheets for cost-effective solar cells. *InfoMat* 2:975–983. <https://doi.org/10.1002/inf2.12070>
- [31] Greaney MJ, Brutchey RL (2015) Ligand engineering in hybrid polymer: nanocrystal solar cells. *Mater Today* 18:31–38. <https://doi.org/10.1016/j.mattod.2014.07.004>
- [32] Tiwari A, Dhoble SJ, Kher RS (2015) Influence of thiol capping on the photoluminescence properties of L-cysteine-, mercaptoethanol- and mercaptopropionic acid-capped ZnS nanoparticles. *Luminescence* 30:1148–1152. <https://doi.org/10.1002/bio.2877>
- [33] Kumar S, Scholes GD (2008) Colloidal nanocrystal solar cells. *Microchim Acta* 160:315–325. <https://doi.org/10.1007/s00604-007-0806-z>
- [34] Oreggioni DA, Aguiar I, Fornaro L, Pérez ME (2018) Hydrothermal synthesis and characterization of SnS₂ nanoparticles with capping pyridine and aniline. *MRS Adv* 3:2–7. <https://doi.org/10.1557/adv.2018>
- [35] Verma VK, Singh Y, Chauhan RN et al (2010) Characterization of CdSe nanocrystals for hybrid solar cells. *Integr Ferroelectr* 120:1–5. <https://doi.org/10.1080/10584587.2010.491010>
- [36] Ananthakumar S, Ramkumar J, Moorthy Babu S (2014) Effect of ligand exchange in optical and morphological properties of CdTe nanoparticles/P3HT blend. *Sol Energy* 106:151–158. <https://doi.org/10.1016/j.solener.2014.01.046>
- [37] Ghosh SK, Perla VK, Mallick K (2020) Organic molecule stabilized bismuth iodide nanoparticles: a hybrid system with multifunctional physical properties. *Phys Chem Chem Phys* 22:3345–3351. <https://doi.org/10.1039/C9CP06183E>
- [38] Perla VK, Ghosh SK, Mallick K (2020) Aminobenzene stabilized bismuth halide nanoparticles with O-shaped hysteresis behaviour. *J Mater Sci Mater Electron* 31:22652–22661. <https://doi.org/10.1007/s10854-020-04777-7>
- [39] Ali HE, Khairy Y (2020) Facile synthesis, structure, AFM, thermal, and optical analysis of BiI₃/PVAL nanocomposite films for laser CUT-OFF optical devices. *Vacuum* 180:109640. <https://doi.org/10.1016/j.vacuum.2020.109640>
- [40] Zhou Y, Riehle FS, Yuan Y et al (2010) Improved efficiency of hybrid solar cells based on non-ligand-exchanged CdSe quantum dots and poly(3-hexylthiophene). *Appl Phys Lett* 96:013304. <https://doi.org/10.1063/1.3280370>
- [41] Zhang J, Han Q, Wang X et al (2016) Synthesis of δ-Bi₂O₃ microflowers and nanosheets using CH₃COO(BiO) self-sacrifice precursor. *Mater Lett* 162:218–221. <https://doi.org/10.1016/j.matlet.2015.10.024>
- [42] Ahrlund S, Grenthe I (1957) The stability of metal halide complexes in aqueous solution—III. The chloride, bromide and iodide complexes of bismuth. *Acta Chem Scand* 11:1111–1130
- [43] Lide D (2006) *CRC handbook of chemistry and physics*. CRC Press/Taylor and Francis Group, Boca Raton
- [44] The IUPAC Stability Constants Database, SC-Database. <https://www.acadsoft.co.uk>. Accessed 11 Oct 2021
- [45] Kandanapitiye MS, Gao M, Molter J et al (2014) Synthesis, characterization, and X-ray attenuation properties of ultra-small BiOI nanoparticles: toward renal clearable particulate CT contrast agents. *Inorg Chem* 53:10189–10194. <https://doi.org/10.1021/ic5011709>

- [46] Pretsch E, Bühlmann P, Badertscher M (2009) IR spectroscopy BT—structure determination of organic compounds: tables of spectral data. Springer, Berlin, pp 1–67
- [47] Chapel A, Ben DS, Therias S et al (2016) Effect of ZnO nanoparticles on the photochemical and electronic stability of P3HT used in polymer solar cells. *Sol Energy Mater Sol Cells* 155:79–87. <https://doi.org/10.1016/j.solmat.2016.04.052>
- [48] Tremel K, Ludwigs S (2014) Morphology of P3HT in thin films in relation to optical and electrical properties. *Adv Polym Sci* 265:39–82. https://doi.org/10.1007/12_2014_288
- [49] Benchaabane A, Ben Hamed Z, Sanhoury MA et al (2016) Influence of nanocrystal concentration on the performance of hybrid P3HT:TBPO-capped CdSe nanocrystal solar cells. *Appl Phys A Mater Sci Process* 122:1–10. <https://doi.org/10.1007/s00339-015-9572-7>
- [50] Clark J, Silva C, Friend RH, Spano FC (2007) Role of intermolecular coupling in the photophysics of disordered organic semiconductors: aggregate emission in regioregular polythiophene. *Phys Rev Lett* 98:206406. <https://doi.org/10.1103/PhysRevLett.98.206406>
- [51] Dowland SA, Reynolds LX, Maclachlan A et al (2013) Photoinduced electron and hole transfer in CdS:P3HT nanocomposite films: effect of nanomorphology on charge separation yield and solar cell performance. *J Mater Chem A* 1:13896–13901. <https://doi.org/10.1039/c3ta12962d>
- [52] Molefe FV, Khenfouch M, Dhlamini MS, Mothudi MB (2017) Spectroscopic investigation of charge and energy transfer in P3HT/GO nanocomposite for solar cell applications. *Adv Mater Lett* 8:246–250. <https://doi.org/10.5185/a/mllett.2017.1409>
- [53] Kabongo GL, Mbule PS, Mhlongo GH et al (2016) Photoluminescence quenching and enhanced optical conductivity of P3HT-derived Ho^{3+} -doped ZnO nanostructures. *Nanoscale Res Lett* 11:1–11. <https://doi.org/10.1186/s11671-016-1630-3>
- [54] Spano FC (2005) Modeling disorder in polymer aggregates: the optical spectroscopy of regioregular poly(3-hexylthiophene) thin films. *J Chem Phys* 122:234701. <https://doi.org/10.1063/1.1914768>
- [55] Ananthakumar S, Ramkumar J, Moorthy Babu S (2014) Synthesis of thiol modified CdSe nanoparticles/P3HT blends for hybrid solar cell structures. *Mater Sci Semicond Process* 22:44–49. <https://doi.org/10.1016/j.mssp.2014.02.008>
- [56] Singh A, Dey A, Iyer PK (2017) Influence of molar mass ratio, annealing temperature and cathode buffer layer on power conversion efficiency of P3HT:PC71BM based organic bulk heterojunction solar cell. *Org Electron* 51:428–434. <https://doi.org/10.1016/j.orgel.2017.09.036>
- [57] Shalu C, Yadav N, Bhargava K et al (2018) All organic near ultraviolet photodetectors based on bulk hetero-junction of P3HT and DH6T. *Semicond Sci Technol* 33:095021. <https://doi.org/10.1088/1361-6641/aad8d5>
- [58] Maaz K, Karim S, Usman M et al (2010) Effect of crystallographic texture on magnetic characteristics of cobalt nanowires. *Nanoscale Res Lett* 5:1111–1117. <https://doi.org/10.1007/s11671-010-9610-5>
- [59] Brinkmann M, Wittmann JC (2006) Orientation of regioregular poly(3-hexylthiophene) by directional solidification: a simple method to reveal the semicrystalline structure of a conjugated polymer. *Adv Mater* 18:860–863. <https://doi.org/10.1002/adma.200501838>
- [60] Tanaka S, Rosli SKB, Takada K et al (2017) Effects of bromination of poly(3-hexylthiophene) on the performance of bulk heterojunction solar cells. *RSC Adv* 7:46874–46880. <https://doi.org/10.1039/c7ra07454a>
- [61] Wang W, Chen C, Tollan C et al (2017) Efficient and controllable vapor to solid doping of the polythiophene P3HT by low temperature vapor phase infiltration. *J Mater Chem C* 5:2686–2694. <https://doi.org/10.1039/C6TC05544C>
- [62] Colle R, Grosso G, Ronzani A, Zicovich-Wilson CM (2011) Structure and X-ray spectrum of crystalline poly(3-hexylthiophene) from DFT-van der Waals calculations. *Phys Status Solidi* 248:1360–1368. <https://doi.org/10.1002/pssb.201046429>
- [63] Jouane Y, Colis S, Schmerber G et al (2012) Annealing treatment for restoring and controlling the interface morphology of organic photovoltaic cells with interfacial sputtered ZnO films on P3HT:PCBM active layers. *J Mater Chem* 22:1606–1612. <https://doi.org/10.1039/C1JM13569D>
- [64] Sugiyama K, Kojima T, Fukuda H et al (2008) ESR and X-ray diffraction studies on thin films of poly-3-hexylthiophene: molecular orientation and magnetic interactions. *Thin Solid Films* 516:2691–2694. <https://doi.org/10.1016/j.tsf.2007.04.067>
- [65] Kleinhenz N, Persson N, Xue Z et al (2016) Ordering of poly(3-hexylthiophene) in solutions and films: effects of fiber length and grain boundaries on anisotropy and mobility. *Chem Mater* 28:3905–3913. <https://doi.org/10.1021/acs.chemmater.6b01163>

Publisher's Note Springer Nature remains neutral with regard to jurisdictional claims in published maps and institutional affiliations.

Springer Nature or its licensor holds exclusive rights to this article under a publishing agreement with the author(s) or other rightsholder(s); author self-archiving of the accepted manuscript version of this article is solely governed by the terms of such publishing agreement and applicable law.